LASER & PHOTONICS REVIEWS

www.lpr-journal.org

Dependence of the Efficiency of the Nonlinear-Optical Response of Materials on their Linear Permittivity and Permeability

Diego M. Solís, Robert W. Boyd,* and Nader Engheta**

The dependence of the efficiency of various nonlinear-optical processes on the background linear relative electric permittivity ϵ and magnetic permeability μ of the material is analytically and numerically investigated. The conversion efficiency of low-order harmonic-generation processes, as well as the increase rate of Kerr-effect nonlinear phase shift and nonlinear losses from two-photon absorption (TPA), are seen to increase with decreasing ϵ and/or increasing μ. The rationale and physical insights behind this nonlinear response are also discussed, particularly its enhancement in ϵ-near-zero (ENZ) media. This behavior is consistent with the experimental observation of intriguingly high effective nonlinear refractive indices in degenerate semiconductors such as indium tin oxide and aluminum oxide (where the nonlinearity is attributed to a modification of the energy distribution of conduction-band electrons due to laser-induced electron heating) at frequencies with vanishing real part of the linear permittivity. Such strong nonlinear response can pave the way for a new paradigm in nonlinear optics with much higher conversion efficiencies and therefore better miniaturization capabilities and power requirements for next-generation integrated nanophotonics. It is concluded that the major contribution to the enhanced nonlinear response of ENZ materials arises from propagation effects, that is, the appearance of ϵ and μ in the reduced wave equation describing the interaction.

1. Introduction

Many research endeavors have focused on the quest for materials with strong and fast nonlinear light–matter interactions. Large ultrafast nonlinear optical responses are paramount for a plethora of applications relying on active photonic integrated circuits, ranging from all-optical signal processing[1,2] to quantum computers.[3,4] But the integration density of these devices, if based on nonresonant nonlinear processes (hinging upon virtual transitions and ergo very fast), is burdened by the intrinsic perturbative nature of such nonlinear phenomena, which typically require high optical intensities and/or long interaction lengths. In order to circumvent this weak response, diverse alternatives have been proposed, aimed at extrinsically boosting nonlinearities with tailored electromagnetic resonances by means of structuring materials, like micro-cavities,[5] slow-light photonic-crystal waveguides,[6,7] metallo-dielectric composites,[8] or plasmonic nanostructures.[9–11]

Moreover, materials with near-vanishing permittivity, known as ϵ-near-zero (ENZ) materials, were initially predicted[12–17] (by virtue of either electric field enhancement or better phase-matching) and later observed[18–29] to enhance nonlinear processes. More recently, transparent conductive oxides (TCOs) such as indium tin oxide (ITO) and Al-doped ZnO (AZO) have drawn much attention as promising candidates to increase the strength of nonlinear interactions. These degenerately doped semiconductors i) are complementary metal-oxide-semiconductor (CMOS)-compatible, ii) have an ENZ wavelength in the near-IR (tuned by varying post-deposition annealing time and temperature) for which the nonlinear refractive index has been experimentally measured to be unprecedentedly large[22,23]—up to several orders of magnitude larger than the previously reported largest value (As_2Se_3 glass)[30]—and with a sub-picosecond response time, and iii) provide less loss than noble metals in this spectral region. In fact, the nonlinear response of these materials is so large that one might question whether the usual expansion of the material polarization as a power series

D. M. Solís, N. Engheta
Department of Electrical and Systems Engineering
University of Pennsylvania
Philadelphia, PA 19104, USA
E-mail: marsolis@seas.upenn.edu; engheta@seas.upenn.edu

R. W. Boyd
Department of Physics
University of Ottawa
Ottawa, Ontario K1N 6NS, Canada
E-mail: boyd@optics.rochester.edu

R. W. Boyd
Institute of Optics and Department of Physics and Astronomy
University of Rochester
Rochester, NY 14627, USA

The ORCID identification number(s) for the author(s) of this article can be found under https://doi.org/10.1002/lpor.202100032

DOI: 10.1002/lpor.202100032

in electric field[31] is still valid. As pointed out in [32], there may still be a convergent power series for the polarization in terms of the electric field amplitude in this regime, although the widely used expression for the intensity-dependent refractive index[31] $n = n_0 + n_2 I$ (n_0 being the linear refractive index, $n_2 = \frac{3\chi^{(3)}}{4n_0 \mathrm{Re}\{n_0\}\epsilon_0 c}$ the nonlinear coefficient, $\chi^{(3)}$ the third-order nonlinear susceptibility, and I the optical intensity), stems from a Taylor expansion that under ENZ conditions is divergent and should therefore be reassessed. Thus the dependence of n on I is non-perturbative, even though the dependence of the polarization on field strength remains perturbative.

Importantly, although the origin of the nonlinear response in ENZ media has been explained semi-classically with electron band theory in refs. [22, 24, 33–36]—the laser induces a temperature rise of free electrons, which lowers the temperature-dependent electron chemical potential of TCOs' nonparabolic conduction band and, in turn, reduces the plasma frequency ω_p in the Drude model, thereby effectively increasing the dielectric function—it appears that the enhanced nonlinear response near the ENZ frequency is purely extrinsic and mainly attributed to the electric-field enhancement[22,24,33] and slow-light effects.[35,36]

Following this spirit, in this manuscript, the theoretical analysis of wave propagation in a nonlinear medium with second- or third-harmonic, instantaneous (nondispersive) susceptibilities is revisited, and the dependence of the nonlinear response on the linear part of the relative dielectric permittivity ϵ, which is allowed to be dispersive, is studied in detail. For the sake of completeness, the variation of linear relative magnetic permeability μ is also taken into account. Furthermore, finite-difference time-domain (FDTD)[37] and frequency-domain (FDFD)[38] full-wave electromagnetic solvers have been implemented (generalized for dispersive media and for arbitrary nonlinear phenomena) to validate the theoretical predictions. It is shown that phase-matched nonlinear propagation has a conversion efficiency that tends to increase with decreasing ϵ and/or increasing μ, because the inverse of the conversion length tends to increase with an increasing relative impedance $\eta = \sqrt{\mu/\epsilon}$. Additionally, the intensity of the reflected second/third harmonics tends to increase with decreasing ϵ and/or μ for normal incidence from vacuum to a semi-infinite region of such nonlinear media. When phase-mismatch is brought into play, it is well-known that destructive interference inhibits the harmonic conversion process and a characteristic space-periodic pattern shows up; it is shown that the maxima of these periodic oscillations either increase with μ and/or $1/\epsilon$, or remain constant but with a spatial frequency that is roughly proportional to the same factor $\sqrt{\mu/\epsilon}$, so the effective conversion length is reduced as ϵ (μ) decreases (increases). We will also connect this η-dependence observed in harmonic-generation processes with the fact that the second-order index of refraction and the two-photon absorption (TPA) coefficient increase with increasing η as well. Finally, we briefly go over the more realistic dispersive nonlinear susceptibilities that emerge from the above-mentioned nonparabolicity.

2. Theory and Numerical Results

For simplicity and without loss of generality, let us focus our description (we herein extend the analytical framework in refs. [31, 39] to include the effect of linear magnetic permeability) on second-harmonic generation within a medium that is lossless at the fundamental and second-harmonic frequencies, ω_1 and $\omega_2 = 2\omega_1$, respectively. We consider plane-wave propagation in the $+z$ direction and express $\tilde{E}_j$, the electric field at frequency ω_j (j=1,2), as

$$\tilde{E}_j(z,t) = 2\mathrm{Re}\left[E_j(z)e^{-i\omega_j t}\right] = 2\mathrm{Re}\left[A_j(z)e^{i(k_j z-\omega_j t)}\right] \tag{1}$$

where a slowly varying complex amplitude $A_j(z)$ is used, and $k_j = n_j\frac{\omega_j}{c}$ is the wavenumber, with $n_j = \sqrt{\mu_j\epsilon_j}$ the refractive index, μ_j and ϵ_j being the linear relative permeability and permittivity at frequency ω_j, respectively. The presence of nonlinear polarization $\tilde{P}_{NL,j}$ leads to the following well-known inhomogeneous wave equation for $\tilde{E}_j$[31]:

$$\frac{\partial^2\tilde{E}_j(z,t)}{\partial z^2} - \frac{\mu_j\epsilon_j}{c^2}\frac{\partial^2\tilde{E}_j(z,t)}{\partial t^2} = \frac{\mu_j}{c^2\epsilon_0}\frac{\partial^2\tilde{P}_{NL,j}(z,t)}{\partial t^2} \tag{2}$$

with:

$$\tilde{P}_{NL,1}(z,t) = 2\mathrm{Re}\left[2\epsilon_0 A_2(z)A_1^*(z)\chi^{(2)}e^{i((k_2-k_1)z-\omega_1 t)}\right] \tag{3a}$$

$$\tilde{P}_{NL,2}(z,t) = 2\mathrm{Re}\left[\epsilon_0 A_1^2(z)\chi^{(2)}e^{i(2k_1 z-\omega_2 t)}\right] \tag{3b}$$

where the second-order nonlinear optical susceptibility is denoted by $\chi^{(2)}$. By placing Equations (1) and (3) into Equation (2), and making the slowly varying amplitude approximation (SVAA), $|\frac{d^2A_j}{dz^2}| \ll |k_j\frac{dA_j}{dz}|$, it is straightforward to arrive at the pair of coupled-amplitude equations:

$$\frac{dA_1}{dz} = i\frac{\eta_1\omega_1\chi^{(2)}}{c}A_2(z)A_1^*(z)e^{-i\Delta kz} \tag{4a}$$

$$\frac{dA_2}{dz} = i\frac{\eta_2\omega_2\chi^{(2)}}{2c}A_1^2(z)e^{i\Delta kz} \tag{4b}$$

where $\Delta k = 2k_1 - k_2$. It is convenient to introduce normalized field amplitudes $u_j(z) = \sqrt{I_j(z)/I}$, where $I_j(z) = \frac{2|A_j(z)|^2}{\eta_0\eta_j}$ is the intensity of the j-th harmonic, $\eta_0 = \sqrt{\mu_0/\epsilon_0}$ is the intrinsic impedance of vacuum and $\eta_j = \sqrt{\mu_j/\epsilon_j}$ is the relative impedance. Following the Manley-Rowe relations, the total intensity I is constant, so $\Sigma_j u_j^2 = 1$. If we define a characteristic interaction length

$$l = \frac{c}{\omega_1\chi^{(2)}}\sqrt{\frac{2}{\eta_1^2\eta_2\eta_0 I}} \tag{5}$$

a measure of the normalized phase velocity mismatch will be $\Delta s = \Delta k l$.

2.1. Perfect Phase-Matching

If the phase velocity of both harmonics is the same, we have Δs=0. In this scenario, one can make use of the fact that $u_1(z)^2u_2(z)\cos(\theta(z))$ is a conserved quantity,[31,39] with $\theta = 2\phi_1(z) - \phi_2(z) + \Delta kz$ (ϕ_j being the phase of the complex amplitude A_j),

and use $\Gamma = u_1(0)^2 u_2(0)\cos(\theta(0))$ to decouple Equations (4a) and (4b). After some lengthy mathematical manipulations, and using $\zeta = z/l$,[31,39] one can arrive at an equation expressed only in terms of $u_2(\zeta)$

$$\frac{du_2^2(\zeta)}{d\zeta} = \pm 2\sqrt{u_2^2(\zeta)\left(1-u_2^2(\zeta)\right)^2 - \Gamma^2} \tag{6}$$

whose general solution has the form of the elliptic integral

$$\zeta = \pm\frac{1}{2}\int_{u_2^2(0)}^{u_2^2(\zeta)} \frac{d(u_2^2)}{\sqrt{u_2^2(1-u_2^2)^2 - \Gamma^2}} \tag{7}$$

u_2^2, which oscillates between the two lowest positive roots of the integrand's denominator, can thus be expressed in closed form with the help of the Jacobi elliptic function $sn()$.[40] Nonetheless, assuming $u_2(0)$=0, that is, only the fundamental frequency impinges on the semi-infinitely extended nonlinear medium, the solution is reduced to the simpler form:

$$u_1(\zeta) = \mathrm{sech}(\zeta), \quad u_2(\zeta) = \tanh(\zeta) \tag{8}$$

In terms of these results we can immediately find the intensity and amplitude conversion efficiencies from the ω_1 wave to the ω_2 wave, defined as $\frac{I_2(z)}{I_1(0)}$ and $\frac{|A_2(z)|}{|A_1(0)|}$ respectively, as $u_2^2(z)$ and $u_2(z)$. From inspection of Equation (8), it is thus clear that conversion efficiency increases with increasing l^{-1}, which will vary with $\sqrt{\eta_1^2\eta_2 I_1(0)}$ or, equivalently, with $\sqrt{\eta_1\eta_2}|A_1(0)|$. For the perfect phase-matching condition in an isotropic medium, we need to have $2\omega_1\sqrt{\mu_1\epsilon_1} = \omega_2\sqrt{\mu_2\epsilon_2}$. This can be achieved in several different ways: 1) For non-magnetic isotropic materials where $\mu_1 = \mu_2 = 1$, phase matching occurs when $\epsilon_1 = \epsilon_2$, which is possible when we are far away from any resonance of the material and $\epsilon_1 = \epsilon_2 > 1$. However, near the ENZ frequencies, the permittivity function is dispersive and thus it should be a function of frequency. Therefore, the condition $\epsilon_1 = \epsilon_2$ can be achieved near zero crossing of the dispersion curves at ω_1 and ω_2 with properly engineered materials with two or more Lorentzian dispersions (or one Drude and one or more Lorentzian dispersions); 2) for the case of magnetic isotropic materials, we can have $\epsilon_1 \neq \epsilon_2$ when $\mu_1 \neq \mu_2$ such that $2\omega_1\sqrt{\mu_1\epsilon_1} = \omega_2\sqrt{\mu_2\epsilon_2}$. There are other cases such as anisotropic materials in which the phase-matching condition may occur for a given direction of propagation. Here, for the sake of simplicity, we assume the first case. When $\epsilon = \epsilon_1 = \epsilon_2$ and $\mu = \mu_1 = \mu_2$, we have a stretching/compression of the z-axis by a factor h such that $u_{2,\eta=h}(z) = u_{2,\eta=1}(hz)$ when $A_1(0)$ is fixed, or $u_{2,\eta=h}(z) = u_{2,\eta=1}(\sqrt{h^3}z)$ when $I = I_1(0)$ is fixed (moreover, for small ζ, given that $\tanh(\zeta) \approx \zeta$, the intensity and amplitude conversion efficiencies scale with η^3 and η, respectively). This behavior can be seen in **Figure 1**, which shows the evolution of u_2^2 versus distance (normalized with respect to the wavelength of the fundamental frequency in vacuum λ) for $\chi^{(2)} = 5 \times 10^{-12}$ [m V^{-1}] and different values of $\epsilon = \epsilon_1 = \epsilon_2$ ranging from 0.01 to 100 ($\mu = \mu_1 = \mu_2$ is set to 1), while keeping the electric field amplitude constant (solid lines) or the intensity constant (dashed lines). One can see that identical curves would be obtained by setting ϵ=1 and varying μ from 100 to 0.01. Moreover,

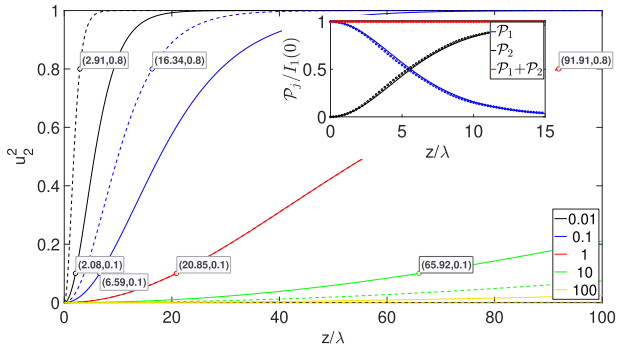

Figure 1. Normalized intensity of the second-harmonic wave as predicted by the analytic solution of Equation (8) versus z/λ for various values of ϵ and for $\chi^{(2)} = 5 \times 10^{-12}$ [m V^{-1}]. Solid lines: fixed $A_1(0) = 5 \times 10^8$ [V m^{-1}] (the data cursors give the values $(z/\lambda, u_2^2)$ at the indicated point and mark the distances at which $u_2^2(z) = 0.1$, illustrating the previously mentioned η z-scaling with η). Dashed lines: fixed $I = 2(5 \times 10^8)^2/\eta_0$, that is, the intensity corresponding to the previous fixed value of $A_1(0)$ when $\epsilon_1 = 1$ (the data cursors mark the distances at which $u_2^2(z) = 0.8$, illustrating now the $\sqrt{\eta^3}$ z-scaling with η). The inset displays, for $\epsilon = 0.01$, the time-averaged Poynting vector $\mathcal{P}_j$ with (solid lines) and without (markers) the SVAA approximation, showing that the SVAA is almost perfectly valid. In this latter case, the initial condition $d^2A_2(0)/dz^2 = 0$ is applied. Note that $\mathcal{P}_j/I_1(0)$ is equal to u_j^2 only when the SVAA approximation is considered, so only $\mathcal{P}_j$, and not u_j^2 as defined so far, can be compared.

the magnetic permeability can be used as an extra degree of freedom to achieve phase-matching, by choosing the permittivities and permeabilities such that $\mu_1\epsilon_1 = \mu_2\epsilon_2$. Crucially, we note that the SVAA approximation loses its validity as $\epsilon\mu$ is reduced (the wavelength increases and thus the term $|k_j\frac{dA_j}{dz}|$ decreases), which in Figure 1 especially concerns the case for which ϵ=0.01. A numerical resolution of the two coupled equations resulting from adding the terms $\frac{d^2A_j}{dz^2}$ to Equations (4a) and (4b) yields, however, time-averaged Poynting vector curves that are very close to the ones obtained with the second of Equation (8) (see inset in Figure 1). If we were to reduce the value of the dielectric function even further, the disagreement between both solutions would be more apparent.

Analagous derivations for third-harmonic generation (considering nonlinear processes characterized by $\chi^{(3)}(3\omega;\omega,\omega,\omega)$ and $\chi^{(3)}(\omega;3\omega,-\omega,-\omega)$) will yield, in the SVAA approximation and considering $\Delta k = 0$ and $u_3(0) = 0$, a closed-form solution of the form

$$u_1(\zeta) = \frac{1}{\sqrt{1+\zeta^2}}, \quad u_3(\zeta) = \frac{\zeta}{\sqrt{1+\zeta^2}} \tag{9}$$

where the characteristic interaction length $l = z/\zeta$ is now defined as:

$$l = \frac{c}{3\omega_1\chi^{(3)}}\frac{4}{\sqrt{\eta_1^3\eta_3\eta_0 I}} \tag{10}$$

The distance scale for conversion of the fundamental to the third harmonic will thus decrease as $\sqrt{\eta_1^3\eta_3 I}$ or, equivalently, as $\sqrt{\eta_1\eta_3}|A_1(0)|^2$. Assuming $\epsilon = \epsilon_1 = \epsilon_3$ and $\mu = \mu_1 = \mu_3$, $u_{3,\eta=h}(z)$

$= u_{3,\eta=1}(hz)$ or $u_{3,\eta=h}(z) = u_{3,\eta=1}(h^2 z)$ will hold when either $A_1(0)$ or I are fixed, respectively. For small ζ, the intensity and amplitude conversion efficiencies thus scale with η^4 and η, respectively.

Let us now study the totality of nonlinear processes arising from such instantaneous (nondispersive) second-order ($P^{(2)}(t) = \epsilon_0 \chi^{(2)} E^2(t)$) and third-order—or Kerr effect— ($P^{(3)}(t) = \epsilon_0 \chi^{(3)} E^3(t)$) nonlinear polarizations. In order to do so, we developed an FDTD algorithm[41,42] incorporating these nonlinear interactions, which naturally cover the entire optical spectrum when described in the time domain (that is, all higher harmonics and their nonlinear interactions are implicitly taken into account). We consider a "half-space" problem (effectively achieved with perfectly matched layers) where an incident plane-wave in vacuum meets the interface with the nonlinear medium with an electric field amplitude normalized such that, regardless of the different values of ϵ considered (from 0.01 to 1), the transmitted electric field immediately on the other side of the interface is kept constant and equal to $E_0 = 2A_1(0) = 10^9$ [V m^{-1}]. Of course, strictly speaking, higher harmonics may already be created in reflection at the interface, so the initial condition $u_{2,3}(0)=0$ assumed in our previous analysis is not, in general, strictly satisfied here anymore[31,43] (see also Equations (19) and (20)); depending on the initial phase difference among these harmonics, they may actually first decrease to zero before steadily increasing.

The numerical results in **Figures 2** and **3**, obtained from FDTD simulations (we note that the reached steady states exhibit long-time stability), very clearly depict the increase of nonlinear response as ϵ is reduced, in agreement with the analytical analysis shown above. It is also interesting to point out that, in normalizing the electric field transmitted through the interface, the transmitted intensity actually decreases with $\sqrt{\epsilon}$. Therefore, if one normalizes transmitted intensity rather than amplitude, the distances in Figure 2a (Figure 3a) will be $1/\sqrt[4]{\epsilon}$ ($1/\sqrt{\epsilon}$) times shorter. This is consistent with the conversion efficiencies previously predicted by our analytic model. Figures 2c and 3c depicting the magnetic field are the most revealing of the underlying physical mechanism explaining this enhancement: for fixed $|A_1(0)|$, assuming not only $\Delta k = 0$ but also a nondispersive medium ($\eta_j = \eta$, $\forall j$) for simplicity, both second- and third-order processes present a conversion efficiency that increases with increasing η, that is, a weaker (in relative terms) magnetic field enhances the nonlinear response. Let us gain some more intuitive insight as to why this is the case. Given that nonlocal effects are not under consideration, it is clear that the (local) nonlinear polarization sees its effect "translated" from time to space through $\nabla \times \mathbf{H}$, according to Maxwell-Ampère's law. For a $\hat{y}$-polarized plane-wave propagating in $+z$ and keeping the adopted $e^{-i\omega t}$ convention, Maxwell's curl equations can be written as

$$\frac{dH_x(z,\omega_j)}{dz} = -i\omega_j\left(\epsilon_0 \epsilon E_y(z,\omega_j) + P_{y,NL}(z,\omega_j)\right) \tag{11a}$$

$$H_x(z,\omega_j) = -\frac{1}{i\omega_j \mu_0 \mu}\frac{d}{dz}\left(A_{y,j}(z)e^{ik_j z}\right) \approx -\frac{k_j}{\omega_j \mu_0 \mu}A_{y,j}(z)e^{ik_j z} \tag{11b}$$

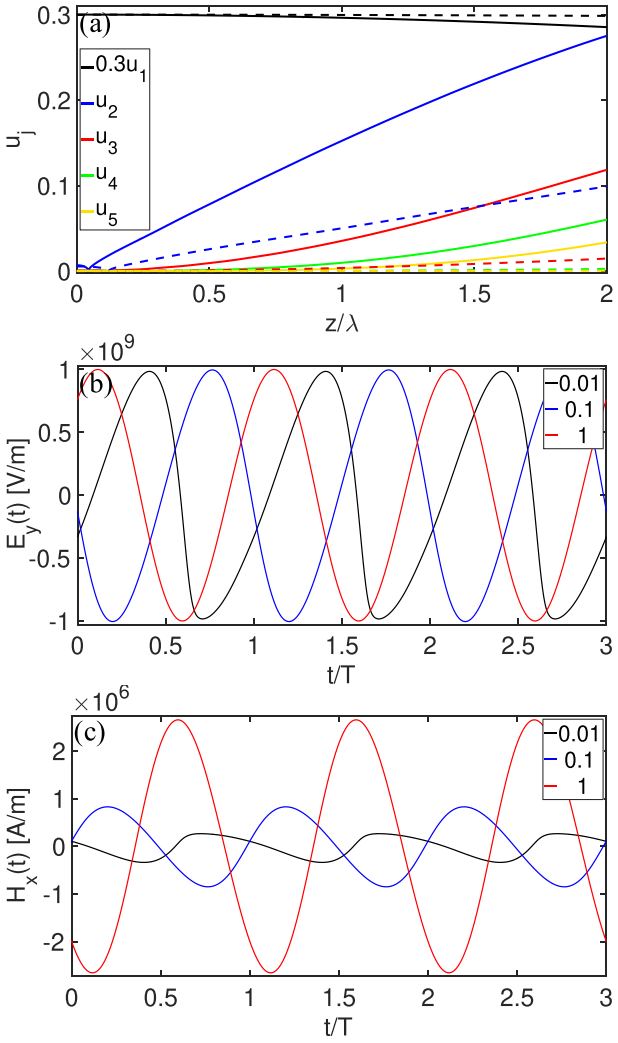

Figure 2. Second-order nonlinear response obtained through FDTD simulations. a) Normalized field amplitudes of the first five harmonics for ϵ = 0.01 and 0.1 (solid and dashed lines, respectively) versus depth normalized to the vacuum wavelength into the nonlinear medium. b,c) Temporal variation of the electric and magnetic fields at a distance of two vacuum wavelengths of the fundamental wave from the interface, for different values of ϵ. Comparison of panels (b) and (c) seems to suggest that H_x displays more distortion than E_y, which is consistent with the additional distortion coming from the term $\frac{dA_{y,j}(z)}{dz}$ in $H_x(z,\omega_j) = -\frac{1}{i\omega_j\mu_0\mu}(ik_j A_{y,j}(z) + \frac{dA_{y,j}(z)}{dz})e^{ik_j z}$. However, this augmented distortion in H_x is much less pronounced than it seems from visual inspection, and is mostly owed to the ratio of the horizontal and vertical axes (i.e., if both E_y and H_x are normalized to 1, their distortions look very similar).

where $\frac{dA_{y,j}(z)}{dz}$ has been neglected in the second form of Equation (11b) under the assumption, again, that the envelope $A_{y,j}(z)$ is slow-varying. A measure of the effective increase in nonlinear distortion with respect to distance felt by the j-th harmonic could be written as

$$\frac{\left|\left[\frac{dH_j(z)}{dz}\right]_{NL}\right|}{|H_j(z)|} \approx \frac{|\omega_j P_{NL,j}(z)|}{|\frac{k_j}{\omega_j\mu_0\mu}A_j(z)|} = \omega_j \eta_0 \eta \frac{|P_{NL,j}(z)|}{|A_j(z)|} \tag{12}$$

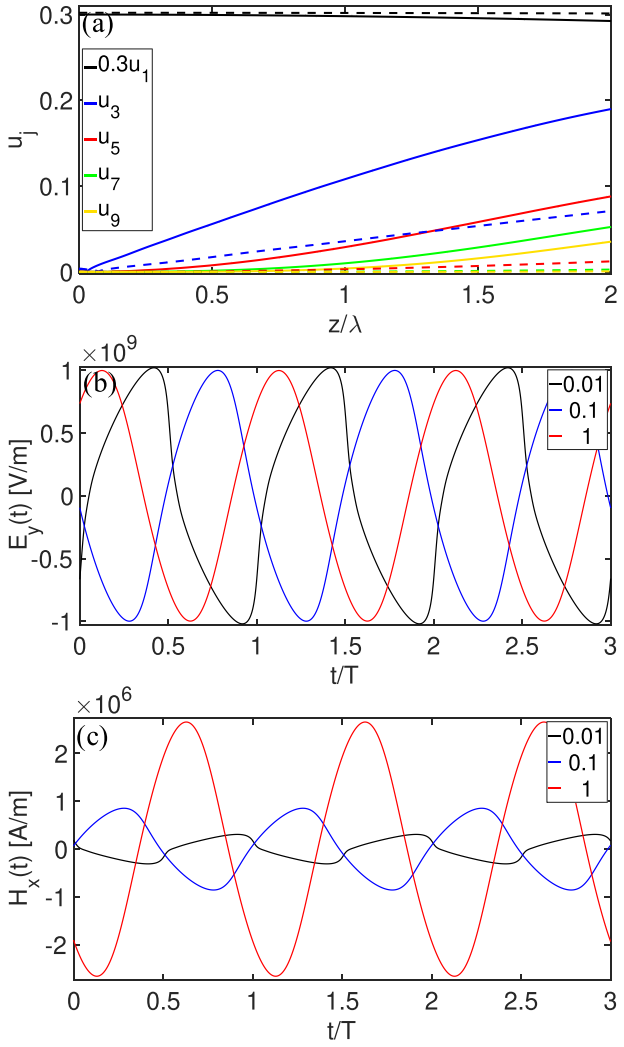

Figure 3. Third-order nonlinear response calculated numerically with FDTD. a–c) Same as in Figure 2, but with $\chi^{(3)} = \chi^{(2)}/E_0 = 5 \times 10^{-21}$ [(m V^{-1})^2].

As expected, the factor η shows up again. Otherwise, this dependence on ϵ is consistent with physical intuition in that nonlinear polarization represents a larger fraction of total polarization as ϵ is reduced. Indeed, Equation (11a) reveals the contributions of the linear and nonlinear portions of the displacement current, demonstrating that in ENZ media the nonlinear part plays a more dominant role even though the coefficients $\chi^{(2)}$ or $\chi^{(3)}$ are kept unchanged.

Furthermore, the temporal evolution of the electric field in the case of instantaneous third-order nonlinear polarization, Figure 3b, has intriguing resemblance with the time-inverted version of the so-called relaxation-oscillations[44] of the Van der Pol nonlinear damped oscillator (well-known in the analysis of circuits containing vacuum tubes), whose oscillation amplitude $x(t)$ obeys the second-order differential equation

$$\frac{d^2x(t)}{dt^2} - \mu\left(1 - x^2(t)\right)\frac{dx(t)}{dt} + x(t) = 0 \tag{13}$$

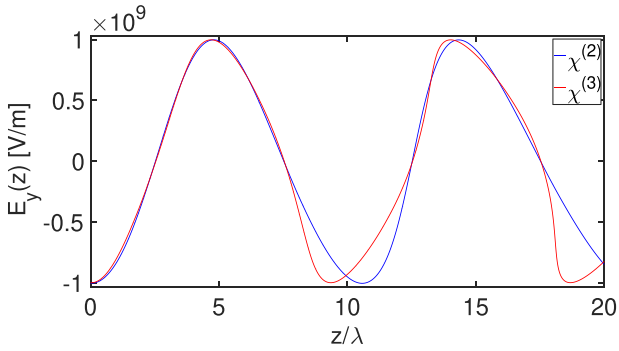

Figure 4. FDTD-simulated electric field versus normalized distance at a given instant in time with $\epsilon = 0.01$, for both second- and third-order polarizations.

For completeness, a time snapshot of the electric field versus z/λ in **Figure 4** shows how the waveforms associated with $\chi^{(2)}$ and $\chi^{(3)}$ processes are increasingly distorted with distance when ϵ=0.01. For visualization purposes, given that the wavelength of the fundamental frequency in the nonlinear medium is in this case ten times the vacuum wavelength, we reduce the rate at which distortion increases with z by decreasing the nonlinear susceptibilities by one order of magnitude with respect to Figures 2 and 3, and we increase the simulation domain accordingly. It is thought-provoking to see that the wavefront originating from the Kerr effect somewhat reminds us of a shockwave. Actually, one might think of taking advantage of this high spatial-frequency content in highly resolved microscopy applications.

2.1.1. Intensity-Dependent Refractive Index

Let us for a moment step back and reflect on how these results on harmonic-generation processes can be connected to the optical Kerr effect and consider only the fundamental frequency ω, in which case the nonlinear polarization can be written as

$$P_{NL}(\omega) = 3\epsilon_0\chi^{(3)}(\omega;\omega,\omega,-\omega)|E(\omega)|^2E(\omega) \tag{14}$$

which yields, in the lossless case, an intensity-dependent refractive index

$$n = n_0 + \Delta n = \sqrt{\mu}\sqrt{\epsilon + 3\chi^{(3)}|E(\omega)|^2} \tag{15}$$

where Δn is the nonlinear change in n and is usually written as $\Delta n = \bar{n}_2|E(\omega)|^2$ or $\Delta n = n_2 I$, with $\bar{n}_2 = \frac{3\eta\chi^{(3)}}{4}$ and $n_2 = \eta_0\eta\bar{n}_2 = \frac{3\eta_0\eta^2\chi^{(3)}}{4}$ correct only to terms of order I[31,32]: importantly, the same factor η that shows up in the conversion efficiency of harmonic-generation processes now arises in the E-dependence of Δn. The rate of phase shift versus distance is therefore $\frac{d\phi}{dz} = (n_0 + \Delta n)\frac{\omega}{c}$, and thus the total nonlinear phase shift as measured in Z-scan experiments[45] is $\Delta n\frac{\omega}{c}L$, where L is the length of the nonlinear medium; perhaps, though, $\frac{\Delta n}{n_0} \approx \frac{3\chi^{(3)}|E(\omega)|^2}{4\epsilon} = \frac{3\eta_0\sqrt{\mu}\chi^{(3)}I}{4\sqrt{\epsilon^3}}$ might represent a better (normalized) measure of nonlinear phase shift. In any case, while it is true that this first-order correction leads to $\bar{n}_2 \to \infty$ or $n_2 \to \infty$ as $\epsilon \to 0$,[32] the fact remains

that $\Delta n = \sqrt{\mu}\sqrt{\epsilon + 3\chi^{(3)}|E(\omega)|^2} - \sqrt{\mu\epsilon}$, which is exact, increases towards the asymptotic value of $\sqrt{3\mu\chi^{(3)}}|E(\omega)|$ as ϵ decreases (this is seen in **Figure 5**a, where we compare the exact value of Δn with its first-order approximation versus ϵ when $\mu = 1$). Consequently, $\frac{\Delta n}{n_0}$ actually tends to ∞. Incidentally, the relative error of the first-order approximation of Δn is approximately constant with μ.

We implemented a nonlinear FDFD full-wave solver so as to see the effect of this nonlinear phase shift numerically. Figure 5b shows the resulting electric field when, instead of a plane-wave, the excitation of our half-space problem is a normally incident paraxial approximation of a Gaussian beam, with a beam waist radius of 4λ, λ being the vacuum wavelength. We choose the setup of this problem to be 2D with TM polarization, and compare the nonlinear results when $\epsilon = 0.1$ and $\epsilon = 1$, showing a larger beam distortion when $\epsilon = 0.1$, as predicted by the theoretical on-axis increase of refractive index: $\Delta n_{\epsilon=0.1} = 0.1021 > \Delta n_{\epsilon=1} = 0.0368$.

2.1.2. Two-Photon Absorption

Analogous considerations apply if we consider the process of two-photon absorption,[31,46] which we can describe also with Equation (14) by making $\chi^{(3)}(\omega;\omega,\omega,-\omega)$ purely imaginary. If $\chi^{(3)}(\omega;\omega,\omega,-\omega)$ is generally complex, Equation (15) becomes

$$n + i\frac{c\alpha}{2\omega} = \sqrt{\mu}\sqrt{\epsilon + 3\chi^{(3)}|E(\omega)|^2} \tag{16}$$

where $\alpha = \alpha_0 + \Delta\alpha = \alpha_0 + \bar{\alpha}_2|E(\omega)|^2$ is the absorption coefficient, with $\bar{\alpha}_2$ the TPA coefficient. Correct to first order in I (and assuming no linear absorption for simplicity), we now have $\bar{\alpha}_2 = \frac{3\eta\omega\mathrm{Im}[\chi^{(3)}]}{2c}$, showing the same η-dependence seen in $\bar{n}_2$.

Similarly as in the previous section, although $\Delta\alpha \to \infty$ (or $\bar{\alpha}_2 \to \infty$ for that matter) as $\epsilon \to \infty$, the exact expression for $\Delta\alpha$ still does increase as ϵ decreases, until reaching the asymptote of value $\frac{2\sqrt{3\mu}\omega\mathrm{Im}[\sqrt{\chi^{(3)}}|E(\omega)|}}{c}$.

2.2. Imperfect Phase-Matching

If the wavevectors are mismatched such that $\Delta s \neq 0$, the integration constant is now $\Gamma + \frac{\Delta s}{2}u_2^2(0)$[39] and Equation (7) is generalized to

$$\zeta = \pm\frac{1}{2}\int_{u_2^2(0)}^{u_2^2(\zeta)} \frac{d(u_2^2)}{\sqrt{u_2^2(1-u_2^2)^2 - \left[\Gamma - \frac{\Delta s}{2}\left(u_2^2 - u_2^2(0)\right)\right]^2}} \tag{17}$$

and u_2 now oscillates according to the solution in [39], expressed in terms of the Jacobi elliptic function $sn()$.[40] For the initial condition of interest $u_2(0) = 0$, u_2 will oscillate between 0 and $1/(\frac{|\Delta s|}{4} + \sqrt{1 + (\frac{|\Delta s|}{4})^2})$. The maximum of u_2 will hence increase with decreasing $|\Delta s|$, which for second-order polarization can be written as

$$\Delta s = \frac{2(n_1 - n_2)}{\chi^{(2)}}\sqrt{\frac{2}{\eta_1^2\eta_2\eta_0 I}} = \frac{2(n_1 - n_2)}{\chi^{(2)}}\frac{1}{\sqrt{\eta_1\eta_2}|A_1(0)|} \tag{18}$$

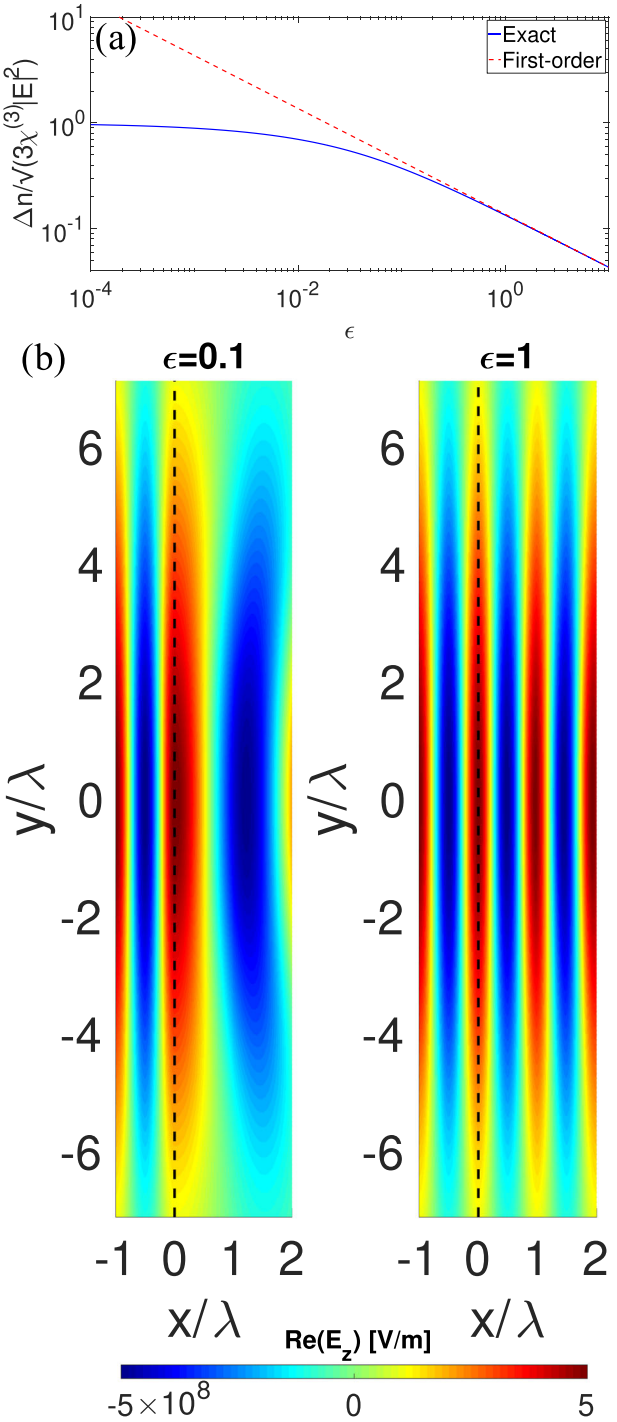

Figure 5. a) Δn (normalized with respect to its asymptotic value when $\epsilon = 0$) versus ϵ. b) Real part of the total electric field phasor obtained from 2D FDFD simulations, for an incoming $\hat{z}$-polarized Gaussian beam at normal incidence with respect to the air/nonlinear medium interface (represented by black dashed lines), with $\epsilon = 0.1$ and $\epsilon = 1$. The incoming electric field is normalized such that $|E(\omega)|_{(x,y)=(0,0)} = A_1(0) = 5 \times 10^8$ [V m^{-1}]. In both panels, $\mu = 1$ and $\chi^{(3)} = 10^{-19}$ [(m V^{-1})^2].

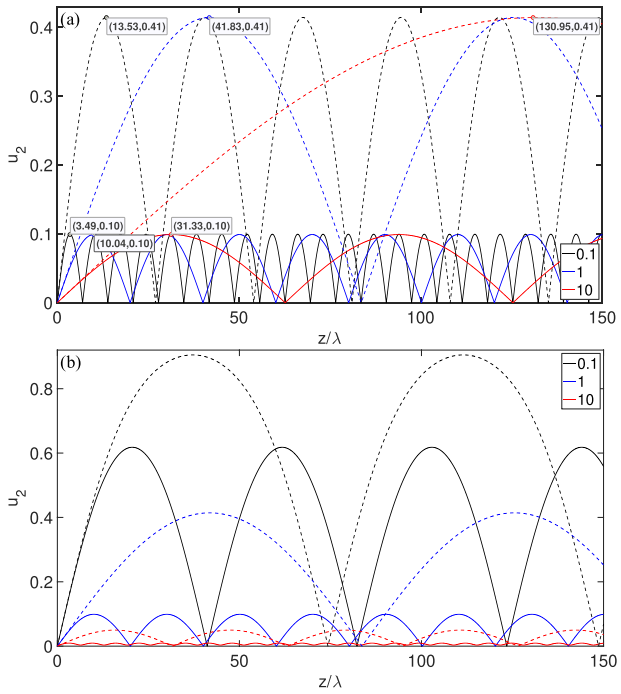

Figure 6. Analytically obtained (the expressions can be found in [39]) normalized field amplitudes of the second harmonic versus normalized depth into the nonlinear medium, with $\epsilon_1 = 0.1$, 1 and 10, for $\epsilon_2 = \epsilon_1 + \Delta$ (panel (a), where the data cursors with XY-pairs $(z/\lambda, u_2)$ mark the first maximum of power conversion for each case) and $\epsilon_2 = \epsilon_1(1 + \Delta)$ (panel (b)). Solid lines: $\Delta = 0.05$ ($\Delta s \approx -20$). Dashed lines: $\Delta = 0.01$ ($\Delta s \approx -4$). The amplitude of the transmitted electric field at the entrance of the nonlinear medium is kept constant: $A_1(0) = 5 \times 10^8$ [V m^{-1}].

Incidentally, note that Δs as defined here will, in general, be a negative number due to Foster's reactance theorem.[47] If we assume there is no magnetic response, $|\Delta s|$ will be proportional to $(\sqrt{\epsilon_1} - \sqrt{\epsilon_2})\sqrt[4]{\epsilon_1\epsilon_2}/|A_1(0)|$. To study the dependence on ϵ_1 and ϵ_2 more fully, we assume that $\epsilon_2 = \epsilon_1 + \Delta$, we fix Δ and vary ϵ_1: we find that $(\sqrt{\epsilon_1} - \sqrt{\epsilon_2})\sqrt[4]{\epsilon_1\epsilon_2}$ is practically constant (this is seen in **Figure 6**a, where the maximum of power conversion is independent of ϵ_1), yet $|\Delta k| \propto |\sqrt{\epsilon_1} - \sqrt{\epsilon_2}|$ decreases with ϵ_1 (i.e., a smaller ϵ_1 will render a larger $|\Delta k|$ but have practically no effect on $|\Delta s|$). With respect to intensity, nevertheless, $|\Delta s| \propto \sqrt[4]{\epsilon_1}$. It is paramount to realize, however, that $A_1(0)$ (or $I = I_1(0)$ for that matter) is referred to the inner side of the vacuum/nonlinear medium interface, so the transmission coefficient, which for normal incidence diminishes with ϵ_1 as $\frac{2}{1+\sqrt{\epsilon_1}}$, plays an important role: conversion efficiency in the nonlinear medium still increases with decreasing ϵ when defined with respect to the incident intensity in vacuum. If we consider, alternatively, $\epsilon_2 = \epsilon_1(1 + \Delta)$, then $|\Delta s| \propto \epsilon_1$, so the maximum of power conversion grows with diminishing ϵ_1, as depicted in Figure 6b.

As expected, the behavior is the opposite if we consider the case in which $\epsilon_1 = \epsilon_2 = 1$ and vary $\mu_{1,2}$. For $\mu_2 = \mu_1 + \Delta$, $|\Delta s|$ grows with diminishing μ_1, whereas for $\mu_2 = \mu_1(1 + \Delta)$, $\frac{\sqrt{\mu_1} - \sqrt{\mu_2}}{\sqrt[4]{\mu_1\mu_2}}$ is a constant equal to $\frac{1-\sqrt{1+\Delta}}{\sqrt[4]{1+\Delta}}$ (with respect to I, $|\Delta s| \propto 1/\sqrt[4]{\mu_1}$). The transmission coefficient for normal incidence will now grow with μ_1 as $\frac{2\sqrt{\mu_1}}{1+\sqrt{\mu_1}}$.

In addition, although the oscillation period of $u_2(\zeta)$ decreases with increasing $|\Delta s|$,[39] ζ is just a stretched/compressed version of z, so it is easy to see that $u_2(z)$, for fixed Δs, will see its period reduced as ϵ_1 (μ_1) decreases (increases). In other words, when Δs is roughly constant with respect to ϵ_1 ($\epsilon_2 = \epsilon_1 + \Delta$ and $\mu_1 = \mu_2 = 1$) or μ_1 ($\mu_2 = \mu_1(1 + \Delta)$ and $\epsilon_1 = \epsilon_2 = 1$), and assuming that $A_1(0)$ is fixed, the first maximum of power conversion is found at a distance into the medium that roughly scales with $\sqrt{\epsilon_1/\mu_1}$, given that $z \propto \frac{\zeta}{\sqrt{\eta_1\eta_2}|A_1(0)|} \approx \frac{\zeta}{\eta_1|A_1(0)|}$ for sufficiently small Δ. This is illustrated in Figure 6a, where the data cursors mark the position of these maxima.

Having reached this point, it is imperative to note that our FDTD half-space problem in Figures 2–4 is not exactly described, at the inner face of the boundary, by the initial conditions assumed throughout the analytical derivations for propagation in a nonlinear medium. In actuality, weak higher harmonic waves are generated in reflection at the interface. Restricting the problem to second-harmonic generation, and neglecting the $\chi^{(2)}(\omega; 2\omega, -\omega)$ process, the boundary value problem can be easily solved as in [43], whose generalization to account for (linear) magnetic permeability yields the following expression, restricted here to the simplified scenario of normal incidence, for the amplitude of the reflected electric field at the second-harmonic frequency:

$$A_2(0) = \frac{\sqrt{\mu_2}(\sqrt{\mu_1\epsilon_1} - \sqrt{\mu_2\epsilon_2})}{(\sqrt{\mu_2} + \sqrt{\epsilon_2})(-\mu_1\epsilon_1 + \mu_2\epsilon_2)}\chi^{(2)}A_1^2(0) \tag{19}$$

As for the second-harmonic wave transmitted into the nonlinear medium, it can be expressed as the superposition of a plane-wave with wavenumber k_2—general solution to the homogeneous wave equation—and a particular solution to the nonhomogeneous equation, in this case a plane-wave with wavenumber $2k_1$; or in more compact form:

$$E_2(z) = A_2(0)\left[1 - \frac{\sqrt{\mu_2}(\sqrt{\mu_2} + \sqrt{\epsilon_2})}{\sqrt{\mu_1\epsilon_1} - \sqrt{\mu_2\epsilon_2}}(e^{i\Delta kz} - 1)\right]e^{ik_2z} \tag{20}$$

It is clear that $E_2(0)$, obviously equal to the reflected wave's amplitude $A_2(0)$, can be used as initial condition for Equations (4a) and (4b), which do take into account the coupling of $E_2(z)$ into $E_1(z)$ described by $\chi^{(2)}(\omega; 2\omega, -\omega)$. If $\mu_1 = \mu_2 = 1$, and we calculate the limit when $\epsilon_1 \to \epsilon_2$, the above expression has a simplified factor of $-\frac{1}{2(\epsilon_1+\sqrt{\epsilon_1})}$. Similarly, if $\epsilon_1 = \epsilon_2 = 1$, the limit when $\mu_1 \to \mu_2$ is $-\frac{1}{2(1+\sqrt{\mu_1})}$. That is, reducing ϵ not only increases conversion efficiency but also the amplitude of the reflected second-harmonic wave. Interestingly, though, increasing μ increases conversion efficiency but decreases nonlinear reflection. Going back to imperfectly matched phase velocities, it was stated before that for a fixed $\Delta = \epsilon_2 - \epsilon_1$, the maximum of conversion efficiency is independent of ϵ_1. On the contrary, the ratio $\frac{\sqrt{\epsilon_1} - \sqrt{\epsilon_1+\Delta}}{\Delta(1+\sqrt{\epsilon_1+\Delta})}$, and thus $u_2(0) = A_2(0)$, now decreases with ϵ_1. If one realizes that $\theta(0) = \pi$ for real $\chi^{(2)}$, $u_2(0)$ is exactly the lower root of the denominator in Equation (17): without loss, $A_2(0)$ is a negative real number and, for very small z, the term $e^{i\Delta kz} - 1$ is purely imaginary and

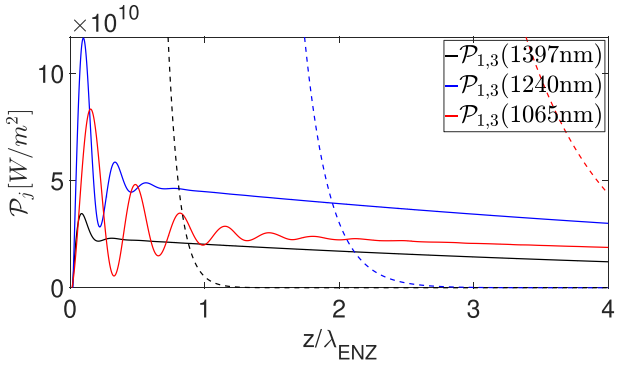

Figure 7. FDTD-calculated time-averaged Poynting vector $\mathcal{P}_j$ for the first (dashed lines) and third (solid lines) harmonic versus distance (normalized with respect to the ENZ wavelength), for different wavelengths of the fundamental, such that $\epsilon_1 = -1.00 + 0.50i$, $0.00 + 0.35i$ and $1.00 + 0.22i$ (black, blue and red, respectively). While the ω_1 wave feels a metallic medium, the ω_3 (and higher harmonics) wave undergoes much lower losses, which allows for propagation. $\mathcal{P}_1$(1065nm) is divided by 50 for visualization.

Table 1. Complex values of the medium's linear permittivity at ω, 3ω and 5ω for the three scenarios of Figure 7, with fundamental wavelengths 1397, 1240, and 1065 nm (black, blue, and red lines, respectively).

	ϵ_1	ϵ_3	ϵ_5
Black	$-1.00 + 0.50i$	$+3.27 + 0.02i$	$+3.61 + 0.00i$
Blue	$+0.00 + 0.35i$	$+3.38 + 0.01i$	$+3.65 + 0.00i$
Red	$+1.00 + 0.22i$	$+3.49 + 0.00i$	$+3.69 + 0.00i$

grows linearly with z; if we match this initial condition at the interface with propagation in the bulk, we have $\phi_2(0) = \pi$ which, assuming $\phi_1(0) = 0$, implies $u_2(0)$ is a minimum. Therefore reducing ϵ_1 can raise the bounds of oscillation of $u_2(z)$.

2.2.1. Lossy Dispersive $\chi^{(1)}$ and Nondispersive $\chi^{(3)}$

The presence of losses in the nonlinear material substantially degrades power conversion. Yet it might be of interest to exploit the dispersion of the linear permittivity to our advantage by centering the fundamental harmonic at a frequency for which the material possesses metallic character but behaves essentially as a dielectric for higher harmonics. This transition region can be found in Drude-type plasmonic materials around the ENZ frequency. In **Figure 7** the time-averaged Poynting vector is depicted versus distance into the unbounded nonlinear half-space, in this case ITO, for $E_0 = 10^9$ [V m^{-1}] (incident intensity of 1.33×10^{15} [W m^{-2}]). The linear dielectric function of ITO is assumed to follow a Drude model with the parameters of [22]: free-electron plasma frequency $\omega_p = 2.9719 \times 10^{15}$ [rad s^{-1}], collision frequency $\gamma = 0.0468\omega_p$, and high-frequency permittivity ϵ_∞=3.8055. These constants fix the ENZ wavelength at 1240 nm. Three wavelengths are considered for the fundamental excitation: 1397, 1240, and 1065 nm, such that Re[ϵ_1] = −1, 0 and 1, respectively (**Table 1** lists all the complex permittivity values for the first three harmonics). A nonlinear susceptibility $\chi^{(3)} = 2 \times 10^{-19}$ [(m V^{-1})^2] is now considered. Figure 7 clearly shows how the third harmonic carries more power than the fundamental after a certain distance, as it

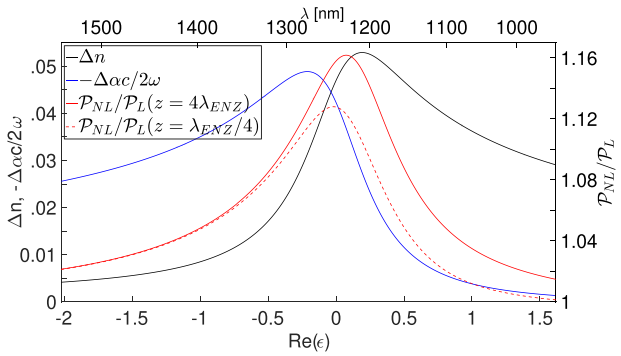

Figure 8. 1D FDFD simulations with the same Drude model as in Figure 7, considering $\chi^{(3)} = 10^{-19}$ [(m V)^2] and an incident electric field of $|E(\omega)| = 5 \times 10^8$ [V m^{-1}]. Δn and $\Delta\alpha$ are depicted versus. Re[ϵ] following the Drude model of parameters indicated above, in the wavelength range of [940, 1540] nm. We also perform linear simulations ($\chi^{(3)} = 0$) and calculate the ratio of nonlinear/linear intensity at $z = 4\lambda_{ENZ}$ (solid red curve in the plot, following a different ordinate axis as indicated on the right-side) and $z = \lambda_{ENZ}/4$ (dashed red curve).

experiences a much lower decay. Notably, the third-harmonic intensity is larger at the ENZ crossing point.

Leaving harmonic generation aside, let us now restrict the discussion to $\chi^{(3)}(\omega;\omega,\omega,-\omega)$ processes only. If we calculate Δn and $\Delta\alpha$ with the dielectric function of the Drude model and use the same $\chi^{(3)}$ as in Figure 5, we get, respectively, the black and blue curves in **Figure 8**. One can see how the maxima of Δn and $\Delta\alpha$ are slightly blue-shifted and red-shifted with respect to the ENZ frequency, respectively. Note also that the plot is showing $-\Delta\alpha$ (more precisely, normalized as the imaginary part of the complex refractive index), that is, the Kerr effect is effectively reducing absorption loss. If we now perform monochromatic nonlinear FDFD simulations with the same Drude parameters of Figure 7, and measure the ratio of nonlinear-to-linear intensity $\frac{\mathcal{P}_{NL}(\omega)}{\mathcal{P}_L(\omega)}$ at two different depths, we obtain the red curves in Figure 8, with maxima of the nonlinear response very close to the ENZ wavelength of 1240 nm. Importantly, these results are perfectly consistent with the experimental observations of an enhanced nonlinear response from ITO thin layers reported in [22, 24]: please note that, although the actual origin of this nonlinearity is ITO's nonparabolic conduction band, one can still define an effective, though dispersive, $\chi^{(3)}$.[35,36]

2.2.2. Realistic Scenario with Both $\chi^{(1)}$ and $\chi^{(3)}$ Dispersive

The mechanism behind the (dispersive) nonlinear susceptibility of TCOs, mentioned above, is extensively studied in [35, 36]: in short, the nonparabolic energy-wavevector ($\mathcal{E} - k$) dispersion relation of ITO's conduction band can be parameterized as $\frac{\hbar^2 k^2}{2m^*} = \mathcal{E} + C\mathcal{E}^2$ (m^* is the free electrons' effective mass at $k = 0$ and C is the nonparabolicity parameter[48]). This gives rise to both virtual and real third-order nonlinear transitions, of anharmonic (instantaneous) and thermal (delayed) nature, respectively. The latter present a nonlinear susceptibility of the order of $\approx 10^{-17}$ [(m V^{-1})$^{-2}$]—roughly two orders of magnitude larger than the former[36]—and are responsible for, for example, ITO's large effective nonlinear refractive index reported near its ENZ

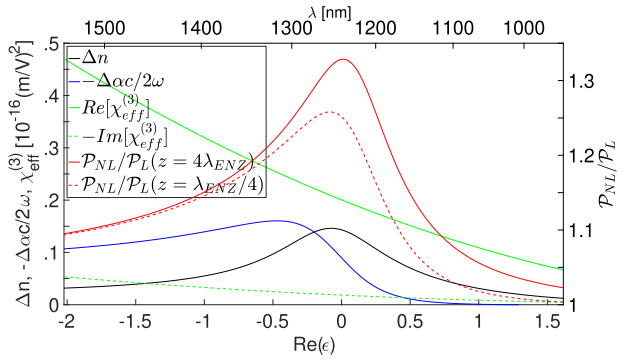

Figure 9. Same scenario as in Figure 8, except we now consider the dispersive nonlinear susceptibility of thermal origin given by Equation (22), with $\tau_{ep} = 100$ fs[36] and m_{eff} equal to 0.4 times the electron mass.[50] This leads to $\chi_t^{(3)} \approx 2\times10^{-17}$ [(m V^{-1})^2] at the ENZ frequency (green solid line), so the incident intensity is reduced by a factor of 10 with respect to Figure 8 in order to keep the nonlinear polarizations of roughly the same order of magnitude.

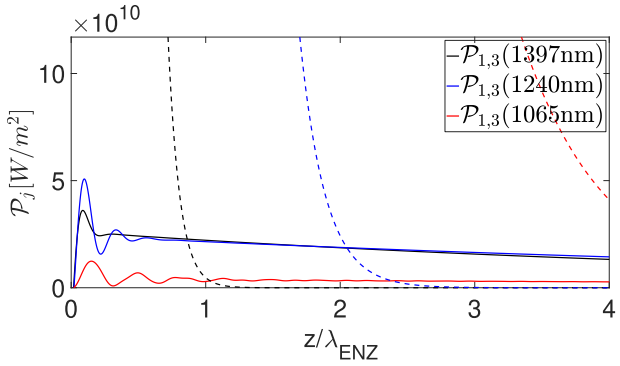

Figure 10. Same scenario as in Figure 7, but considering the dispersive nonlinear susceptibility of quasi-instantaneous nature given by Equation (24).

frequency.[22] This is explained by an increase in the effective mass of the thermalized free carriers promoted above the Fermi level due to optically induced absorption. In the case of degenerately doped TCOs like ITO, it is possible to go without the delayed two-temperature model[49] in the characterization of the thermal energy density U_t, by approximating the average effective mass of the electron gas m_{eff} as the effective mass at the Fermi level[35,36] under the assumption that the electrons' thermal energy is considerably lessthan the ≈1eV Fermi level ($\kappa = \frac{U_t}{N\mathcal{E}_F} \ll 1$, where N is the electron volumetric density and $\mathcal{E}_F$ is the Fermi energy). We can thus write:

$$\frac{\tilde{U}_t(\mathbf{r},t)}{dt} = \tilde{\mathbf{J}}(\mathbf{r},t)\cdot\tilde{\mathbf{E}}(\mathbf{r},t) - \frac{\tilde{U}_t(\mathbf{r},t)}{\tau_{ep}} \tag{21}$$

with $\mathbf{J}$ the free-carrier polarization current, and τ_{ep} the electron-phonon relaxation time.[36] Correct to first order, the thermalized nonlinear plasma frequency can be approximated as $\omega_{p,t}^2(\mathbf{r},t) \approx \omega_p^2(1-\kappa(\mathbf{r},t))$, which allows to substantiate an effective Kerr susceptibility of

$$\chi_t^{(3)}(\omega;\omega,-\omega,\omega) \approx -2\epsilon_0\chi^{(1)}(\omega)\frac{\gamma\tau_{ep}\omega_p^2}{(\omega^2+\gamma^2)N\mathcal{E}_F} \tag{22}$$

This nonlinear process is exemplified in **Figure 9**, which complements the numerical experiment of Figure 8 by replacing an arbitrary instantaneous $\chi^{(3)}$ with the more realistic situation of Equations (21) and (22). The strength of this thermal process leads to even higher nonlinear-to-linear transmission ratios than before with as much as 10 times less laser intensity. The introduction of nonlinear dispersion (see green curves), though evident from the tilt of these ratios (red curves) with respect to the previous ones, still places the peak at the ENZ point.

In addition, the numerous reports of enhanced harmonic generation from thin TCO films excited with obliquely incident TE-polarized light at the ENZ frequency[19,21,25–28] can only be explained through anharmonic nonlinear interactions. We now take a look at these from a purely classical heuristic perspective and draw a parallelism with the Lorentz model of bound electrons subject to a nonparabolic centrosymmetric restoring force.[31] From the $\mathcal{E}$-k dispersion written previously, the kinetic energy of the free electron in the Drude model can be derived as $\mathcal{E} = \frac{-1+\sqrt{1+2Cm\dot{\tilde{x}}^2}}{2C}$ (with $\tilde{x}$ the free electron's displacement), which leads to a force $F = \frac{m\ddot{\tilde{x}}}{\sqrt{1+2Cm\dot{\tilde{x}}^2}}$ or, keeping only the first nonlinear term in the Taylor expansion in $\dot{\tilde{x}}$, $F = m\ddot{\tilde{x}}(1-Cm\dot{\tilde{x}}^2)$. The equation of motion of the free electron's position can then be cast as

$$m\ddot{\tilde{x}}(1-Cm\dot{\tilde{x}}^2) + m\gamma\dot{\tilde{x}} = q\tilde{E}(t) \tag{23}$$

with q the electron charge. In analogy with the thermal nonlinearity, we now have an anharmonic nonlinear plasma frequency $\omega_{p,a}^2(\mathbf{r},t) \approx \omega_p^2(1+Cm(\frac{\tilde{J}(\mathbf{r},t)}{qN})^2)$, where $\gamma = 0$ is assumed for simplicity, which gives rise to the cubic anharmonic susceptibility

$$\chi_a^{(3)}(3\omega;\omega,\omega,\omega) \approx -4\chi^{(1)}(3\omega)Cm\left(\frac{i\omega\epsilon_0\chi^{(1)}(\omega)}{qN}\right)^2 \tag{24}$$

Taking $C = 0.4191$ [eV^{-1}] from [50], we obtain $\chi_a^{(3)} \approx \{2.10-0.51i, 1.32-0.28i, 0.72-0.13i\}\times10^{-19}$ [(m V^{-1})^2] at {1397, 1240, 1065} nm, respectively. These numbers are consistent with the dispersion from the band-theory analysis in [36], proportional to $\frac{1}{3\omega(\omega+i\gamma)^3}$. With these values, we repeat in **Figure 10** the numerical simulations of Figure 7: due to the newly added dispersion, the intensity of the third harmonic is now similar for $\mathrm{Re}[\epsilon_1] = -1$ and $\mathrm{Re}[\epsilon_1] = 0$. But let us not forget that the enhanced ENZ nonlinear response reported in the literature for subwavelength TCO-layers is mainly extrinsic and goes back to the magnification of the normal component of the p-polarized electric field at a given angle, be it by critically coupling the incident transverse wave to the bound plasmon polariton ENZ mode (as in the Kretschmann configuration of [19]) or by exciting the leaky Ferrell–Berreman mode from the longitudinal bulk plasmon resonance (e.g., ref. [21]). A pseudo-Brewster angle with a dip in reflectivity and a peak in absorption can hence be engineered in order to harness the nonlinear response in an extrinsic fashion.

3. Conclusions

We have theoretically shown that the efficiency of the nonlinear response of a material tends to increase with an increasing linear permeability and/or a decreasing linear permittivity, according to a conversion length that decreases with an increasing relative impedance, under phase-matched conditions. We have also seen from Equations (15) and (16) how, in considering the Kerr effect and TPA, this $\sqrt{\mu/\epsilon}$ dependence emerges in the nonlinear change of both the refractive index and the absorption coefficient. Moreover, if wave propagation is phase-mismatched, we have considered two scenarios (we herein restrict the notation to second-harmonic generation): if $\epsilon_2 - \epsilon_1$ ($\mu_2 - \mu_1$) is kept constant, the maximum of power conversion does not vary with ϵ_1 (increases with μ_1) and the oscillation period increases with ϵ_1 (increases with μ_1); if ϵ_2/ϵ_1 (μ_2/μ_1) is kept constant, the maximum of power conversion decreases with ϵ_1 (does not vary with μ_1) and the oscillation period decreases with ϵ_1 (decreases with μ_1). Consequently, either the oscillation amplitude of power conversion tends to increase with increasing μ and/or decreasing ϵ, or else this amplitude stays constant with respect to μ and ϵ, but with an oscillation period that decreases with increasing μ and/or decreasing ϵ.

The behavior described here is consistent with previous experimental measurements of unusually large nonlinear phase shifts of ENZ materials,[22,23] and yet proves that a stronger nonlinear response—restricted in this paper to low-order harmonic-generation processes, Kerr effect and TPA—does not necessarily require a larger nonlinear susceptibility, but can rather be traced back to the relative strengths of the electric and magnetic fields, quantified through the relative impedance. This work thus shows that, even at a fixed value of the nonlinear susceptibility, one can obtain a larger overall nonlinear response, such as an increased conversion efficiency for low-order harmonic generation, by choosing situations such that one or more of the interacting frequencies lies in an ENZ region of the nonlinear material. Finally, we note that under most laboratory conditions the laser intensity has a fixed value, and thus the electric field strength scales as $|E|^2 \propto \sqrt{\mu/\epsilon}I$, which provides an additional mechanism for increasing the efficiency of nonlinear interactions for materials with a large impedance $\sqrt{\mu/\epsilon}$.

Acknowledgements

This work is supported in part by the Defense Advanced Research Projects Agency (DARPA) Defense Sciences Office (DSO) Nascent Light–Matter Interaction program under Grant Number W911NF-18-0369. In addition, R.W.B. acknowledges support from the US Army Research Office through Grant W911NF-18-1-0337.

Conflict of Interest

The authors declare no conflict of interest.

Data Availability Statement

Data sharing is not applicable to this article as no new data were created or analyzed in this study.

Keywords

epsilon-near-zero materials, harmonic generation, indium tin oxide, Kerr effect, nonlinear optics

Received: January 22, 2021
Revised: June 21, 2021
Published online: November 8, 2021

[1] D. Cotter, R. J. Manning, K. J. Blow, A. D. Ellis, A. E. Kelly, D. Nesset, I. D. Phillips, A. J. Poustie, D. C. Rogers, *Science* **1999**, *286*, 1523.
[2] T. D. Vo, H. Hu, M. Galili, E. Palushani, J. Xu, L. K. Oxenløwe, S. J. Madden, D.-Y. Choi, D. A. P. Bulla, M. D. Pelusi, J. Schröder, B. Luther-Davies, B. J. Eggleton, *Opt. Exp.* **2010**, *18*, 17252.
[3] P. G. Kwiat, K. Mattle, H. Weinfurter, A. Zeilinger, A. V. Sergienko, Y. Shih, *Phys. Rev. Lett.* **1995**, *75*, 4337.
[4] J. Leach, B. Jack, J. Romero, A. K. Jha, A. M. Yao, S. Franke-Arnold, D. G. Ireland, R. W. Boyd, S. M. Barnett, M. J. Padgett, *Science* **2010**, *329*, 662.
[5] J. Bravo-Abad, A. Rodriguez, P. Bermel, S. G. Johnson, J. D. Joannopoulos, M. Soljačić, *Opt. Exp.* **2007**, *15*, 16161.
[6] M. Notomi, K. Yamada, A. Shinya, J. Takahashi, C. Takahashi, I. Yokohama, *Phys. Rev. Lett.* **2001**, *87*, 253902.
[7] M. Soljačić, J. D. Joannopoulos, *Nat. Mater.* **2004**, *3*, 211.
[8] N. N. Lepeshkin, A. Schweinsberg, G. Piredda, R. S. Bennink, R. W. Boyd, *Phys. Rev. Lett.* **2004**, *93*, 123902.
[9] G. A. Wurtz, R. Pollard, W. Hendren, G. P. Wiederrecht, D. J. Gosztola, V. A. Podolskiy, A. V. Zayats, *Nat. Nanotechnol.* **2011**, *6*, 107 EP.
[10] W. Cai, A. P. Vasudev, M. L. Brongersma, *Science* **2011**, *333*, 1720.
[11] M. Kauranen, A. V. Zayats, *Nat. Photonics* **2012**, *6*, 737.
[12] A. Ciattoni, C. Rizza, E. Palange, *Phys. Rev. A* **2010**, *81*, 043839.
[13] M. A. Vincenti, D. de Ceglia, A. Ciattoni, M. Scalora, *Phys. Rev. A* **2011**, *84*, 063826.
[14] C. Argyropoulos, P.-Y. Chen, G. D'Aguanno, N. Engheta, A. Alù, *Phys. Rev. B* **2012**, *85*, 045129.
[15] S. Campione, D. de Ceglia, M. A. Vincenti, M. Scalora, F. Capolino, *Phys. Rev. B* **2013**, *87*, 035120.
[16] M. A. Vincenti, D. de Ceglia, J. W. Haus, M. Scalora, *Phys. Rev. A* **2013**, *88*, 043812.
[17] A. Ciattoni, C. Rizza, A. Marini, A. D. Falco, D. Faccio, M. Scalora, *Laser Photonics Rev.* **2016**, *10*, 517.
[18] H. Suchowski, K. O'Brien, Z. J. Wong, A. Salandrino, X. Yin, X. Zhang, *Science* **2013**, *342*, 1223.
[19] T. S. Luk, D. de Ceglia, S. Liu, G. A. Keeler, R. P. Prasankumar, M. A. Vincenti, M. Scalora, M. B. Sinclair, S. Campione, *Appl. Phys. Lett.* **2015**, *106*, 151103.
[20] N. Kinsey, C. DeVault, J. Kim, M. Ferrera, V. M. Shalaev, A. Boltasseva, *Optica* **2015**, *2*, 616.
[21] A. Capretti, Y. Wang, N. Engheta, L. Dal Negro, *ACS Photonics* **2015**, *2*, 1584.
[22] M. Z. Alam, I. De Leon, R. W. Boyd, *Science* **2016**, *352*, 795.
[23] L. Caspani, R. P. M. Kaipurath, M. Clerici, M. Ferrera, T. Roger, J. Kim, N. Kinsey, M. Pietrzyk, A. Di Falco, V. M. Shalaev, A. Boltasseva, D. Faccio, *Phys. Rev. Lett.* **2016**, *116*, 233901.
[24] M. Z. Alam, S. A. Schulz, J. Upham, I. De Leon, R. W. Boyd, *Nat. Photonics* **2018**, *12*, 79.
[25] X. Wen, G. Li, C. Gu, J. Zhao, S. Wang, C. Jiang, S. Palomba, C. Martijn de Sterke, Q. Xiong, *ACS Photonics* **2018**, *5*, 2087.
[26] Y. Yang, J. Lu, A. Manjavacas, T. S. Luk, H. Liu, K. Kelley, J.-P. Maria, E. L. Runnerstrom, M. B. Sinclair, S. Ghimire, I. Brener, *Nat. Phys.* **2019**, *15*, 1022.

[27] W. Tian, F. Liang, S. Chi, C. Li, H. Yu, H. Zhang, H. Zhang, *ACS Omega* **2020**, *5*, 2458.
[28] W. Tian, F. Liang, D. Lu, H. Yu, H. Zhang, *Photon. Res.* **2021**, *9*, 317.
[29] N. C. Passler, I. Razdolski, D. S. Katzer, D. F. Storm, J. D. Caldwell, M. Wolf, A. Paarmann, *ACS Photonics* **2019**, *6*, 1365.
[30] B. J. Eggleton, B. Luther-Davies, K. Richardson, *Nat. Photonics* **2011**, *5*, 141 EP, review Article.
[31] R. W. Boyd, *Nonlinear Optics, Third Edition*, 3rd edition, Academic Press, Inc., Orlando, FL, USA **2008**.
[32] O. Reshef, E. Giese, M. Z. Alam, I. D. Leon, J. Upham, R. W. Boyd, *Opt. Lett.* **2017**, *42*, 3225.
[33] P. Guo, R. D. Schaller, J. B. Ketterson, R. P. H. Chang, *Nat. Photonics* **2016**, *10*, 267.
[34] N. Kinsey, C. DeVault, A. Boltasseva, V. M. Shalaev, *Nat. Rev. Mater.* **2019**, *4*, 742.
[35] R. Secondo, J. Khurgin, N. Kinsey, *Opt. Mater. Exp.* **2020**, *10*, 1545.
[36] J. B. Khurgin, M. Clerici, N. Kinsey, *Laser Photonics Rev.* **2021**, *15*, 2000291.
[37] A. Taflove, S. C. Hagness, *Computational Electrodynamics: The Finite-Difference Time-Domain Method*, Artech House, Boston, MA **2005**.
[38] F. Hildebrand, *Finite-Difference Equations and Simulations*, Prentice-Hall, London, UK **1968**.
[39] J. A. Armstrong, N. Bloembergen, J. Ducuing, P. S. Pershan, *Phys. Rev.* **1962**, *127*, 1918.
[40] E. T. Whittaker, G. N. Watson, *A Course of Modern Analysis*, Cambridge University Press, Cambridge, UK **1996**.
[41] R. M. Joseph, A. Taflove, *IEEE Trans. Antennas Propag.* **1997**, *45*, 364.
[42] C. M. Dissanayake, M. Premaratne, I. D. Rukhlenko, G. P. Agrawal, *Opt. Express* **2010**, *18*, 21427.
[43] N. Bloembergen, P. S. Pershan, *Phys. Rev.* **1962**, *128*, 606.
[44] B. van der Pol Jun. D.Sc, London Edinburgh, and Dublin Philosophical Magazine and Journal of Science **1926**, *2*, 978.
[45] M. Sheik-Bahae, A. A. Said, T.-H. Wei, D. J. Hagan, E. W. Van Stryland, *IEEE J. Quantum Electron.* **1990**, *26*, 760.
[46] G. P. Agrawal, *Nonlinear Fiber Optics*, 5th ed., Academic Press, New York **2012**.
[47] R. M. Foster, *Bell Syst. Tech. J.* **1924**, *3*, 259.
[48] E. O. Kane, *J. Phys. Chem. Solids* **1957**, *1*, 249.
[49] E. Carpene, *Phys. Rev. B* **2006**, *74*, 024301.
[50] X. Liu, J. Park, J.-H. Kang, H. Yuan, Y. Cui, H. Y. Hwang, M. L. Brongersma, *Appl. Phys. Lett.* **2014**, *105*, 181117.